University College Cork, Ireland
Coláiste na hOllscoile Corcaigh

Ku-Band Multi-Functional Bandpass Filtering Isolators (BPFIs) Using GaAs Coupled-Line-Based Unilateral Frequency-Selective Stages

Kexin Li, Andrés Fontana, Dimitra Psychogiou
School of Engineering, University College Cork, Ireland
Tyndall National Institute, Ireland
{kexin.li, andres.fontana}@tyndall.ie, DPsychogiou@ucc.ie

***Abstract*—This paper presents the design and experimental validation of a Ku-band multi-functional RF component integrating the function of a quasi-elliptic bandpass filter and an RF isolator (BPFI). The design is based on cascaded: (i) GaAs MMIC-based unilateral frequency-selective stages (UFSs), comprising a pHEMT transistor-based path and coupled-line feedback, and (ii) passive resonators, whose number and characteristics can be tailored to control the BPFI's selectivity, directivity, and power transmission response. Parametric design studies are conducted to provide insights on UFS characteristic optimization, including gain, bandwidth (BW), noise figure (NF), and input third-order intercept point (IIP3), considering the capabilities of the commercially available 0.15 µm InGaAs process. A coupling routing diagram-based design methodology is also provided, facilitating BPFI design using conventional coupled-resonator synthesis techniques. For experimental validation, a single-stage UFS and a four-stage co-designed BPFI were manufactured and tested using a 0.15 µm GaAs MMIC process. The four-stage BPFI demonstrated a quasi-elliptic transfer function with four poles and three transmission zeros, achieving a passband gain of -1.7 dB, directivity of 30 dB, an NF of 9.2 dB, and an IIP3 of 0.2 dBm at 13 GHz.**

***Keywords*—bandpass filter (BPF), coupled-line filter, isolator, monolithic microwave integrated circuit (MMIC), unilateral filter.**

I. Introduction

Unilateral RF components, such as isolators and circulators, are essential RF front-end (RFFE) elements for emerging joint communication and sensing (JCAS) [1] and in-band full-duplex (IBFD) applications [2]. Particularly, their development for the upcoming FR3 band (7.125-24.25 GHz) will be necessary for enhancing the capacity of existing FR1 networks and enabling new sensing and high-capacity communication systems while maximizing electromagnetic (EM) spectrum utilization. Traditional unilateral components based on ferrite materials [3], rely on large magnets, making them unsuitable for compact integration. Additionally, they primarily focus on isolation performance, requiring extra filters in the RFFE to suppress out-of-band interference.

To tackle the challenges of size and complexity in RFFEs, RF co-design techniques that integrate multiple functionalities into a single RF component are increasingly being explored. Among these, the integration of bandpass filters and isolators (BPFIs) into a single RF component has emerged as a promising solution for effective interference suppression. Various approaches, such as spatiotemporally modulated (STM) resonators and transistor-based designs are considered.

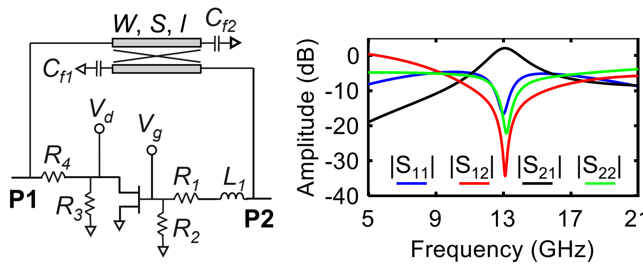

(a) (b)

Fig. 1. UFS. (a) Circuit schematic. (b) Circuit-simulated S-parameters using: V_g = 0.73 V, V_d = 3.3 V, L_1 = 1.1 nH, R_1 = 6 Ω, R_2 = 173 Ω, R_3 = 44 Ω, R_4 = 33.8 Ω, W = 27 µm, S = 37 µm, l = 1387 µm, C_{f1} =0.1 pF, C_{f2} = 0.11 pF.

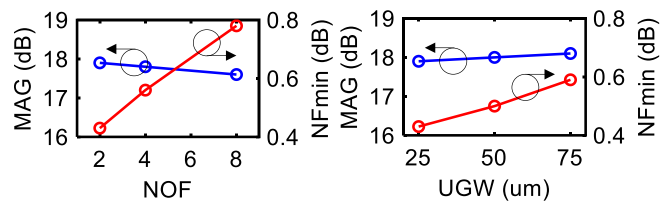

(a) (b)

Fig. 2. Maximum available gain (MAG) and minimum noise figure (NFmin) study of the pHEMT GaAs transistor. Variation of the: (a) Number of fingers (NOF) and (b) Unit gate width (UGW).

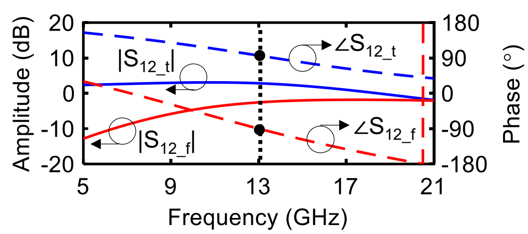

Fig. 3. Circuit-simulated S-parameters of the transistor-based and coupled-line paths for a UFS designed at 13 GHz. S_{12_t}: transistor-based path, S_{12_f}: feedback.

Transistor-based filtering isolators [4] offer commendable performance in terms of gain (4.2–5.8 dB) and isolation (44–71 dB). However, they exhibit high power consumption (e.g., 114.3-228.6 mW [5]). Conversely, STM-based approaches do not consume power but are limited to frequencies below 1 GHz and suffer from significant insertion loss (1.7–6.8 dB) in the forward direction [6], [7].

Considering these limitations, this paper proposes a new implementation scheme for Ku-band BPFIs with a quasi-elliptic power transmission response and directivity exceeding 30 dB, leveraging a commercially 0.15 µm InGaAs process from WIN Semiconductors. The design is based on cascaded unilateral frequency-selective stages (UFSs) [8], [9], [10],

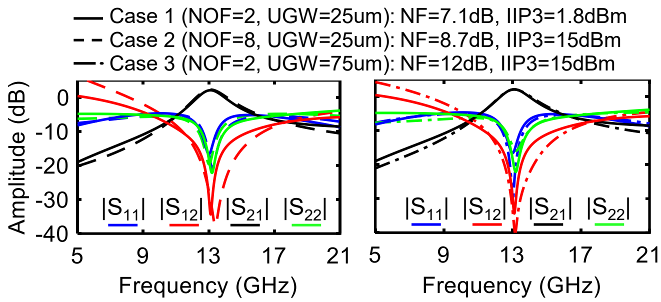

Fig. 4. UFS design cases for different: (a) NOF and (b) UGW of the transistor. Case 1 parameters are listed in the caption of Fig. 1. $V_g = 0.73$ V, $V_d = 3.3$ V in all cases. Case 2:, $L_1 = 0.1$ nH, $R_1 = 38$ Ω, $R_2 = 130$ Ω, $R_3 = 105$ Ω, $R_4 = 40$ Ω, $W = 49$ µm, $S = 33.5$ µm, $l = 1429$ µm. Case 3: $L_1 = 0.5$ nH, $R_1 = 55$ Ω, $R_2 = 59$ Ω, $R_3 = 67$ Ω, $R_4 = 17$ Ω, $W = 28$ µm, $S = 41$ µm, $l = 1360$ µm.

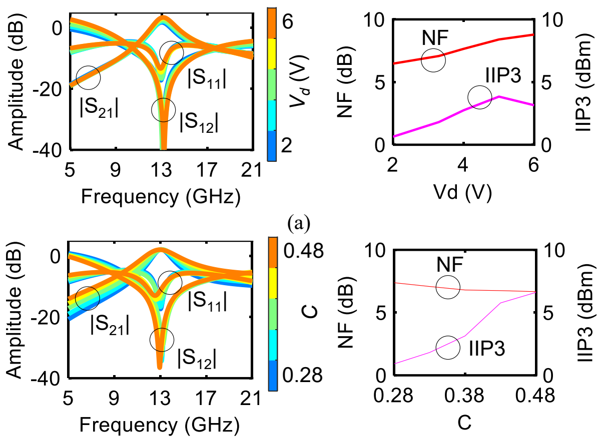

Fig. 5. UFS design cases for different (a) gain and (b) BW. In (a), adjustments to the component values are required to maintain directivity >30 dB when V_d is altered. In (b): the transistor's bias voltage fixed and changes in the coupling factor (C) necessitate component adjustments in the transistor-based path to achieve directivity >30 dB. Parameters omitted for brevity.

combined with passive resonators and mixed EM couplings to enhance the forward-direction selectivity. A comprehensive design methodology utilizing coupling routing diagrams (CRD) is also presented. Parametric design studies including gain, bandwidth (BW), noise figure (NF), and input third-order intercept point (IIP3) are provided to facilitate the UFS design using the 0.15 µm WIN Semiconductor InGaAs process.

II. Theoretical Foundations

A. Unilateral frequency-selective stage (UFS)

To illustrate the BPFI concept, its core component the UFS is first designed for a center frequency (f_{cen}) of 13 GHz. Its circuit schematic is shown in Fig. 1(a), with its design parameters provided in the caption. The UFS consists of two parallel branches: i) a transistor-based branch with the transistor set in a common-source configuration and ii) a capacitive-loaded coupled-line section [10]. Proper amplitude and phase balance at the f_{cen} ensures constructive signal addition in the output in the forward direction and destructive signal cancellation in the reverse [see Fig. 1(b)].

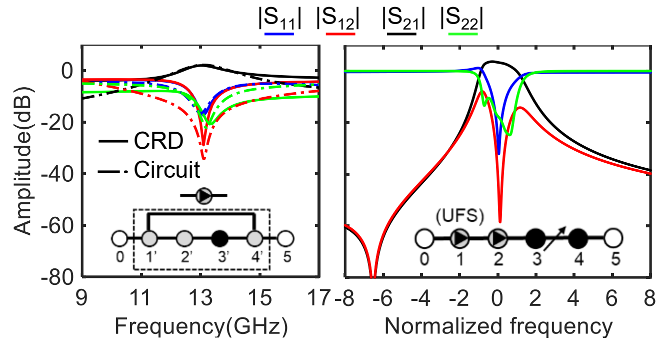

Fig. 6. (a) CRD of the UFS in Fig. 1(a), and comparison between circuit-simulated and CRD-synthesized responses. The coupling coefficients are: $m_{01'} = 1$, $m_{4'5} = 1$, $m_{1'2'} = 1.0998$, $m_{3'4'} = 1.0419$, $m_{2'3'} = 3.3417{+}j0.5754$, $m_{3'2'} = 0.1527{-}j0.0149$, $m_{1'4'} = 1.9908$, $R_{1'1'} = -0.0188{-}j0.0242$, $R_{2'2'} = 1.1945{-}j0.148$, $R_{3'3'} = 1.1735{+}j0.2693$, $R_{4'4'} = 0.1011{+}j0.0947$. (b) CRD and CRD-synthesized response of the four-stage BPFI. The coupling coefficients of the UFS are from (a), the rest are selected as follows: $m_{01} = 0.88$, $m_{12} = 1.2$, $m_{23} = 0.73$, $m_{34} = m'_{34}{+}m''_{34}$ Ω $= 0.85{+}0.13$ Ω, $m_{45} = 0.94$.

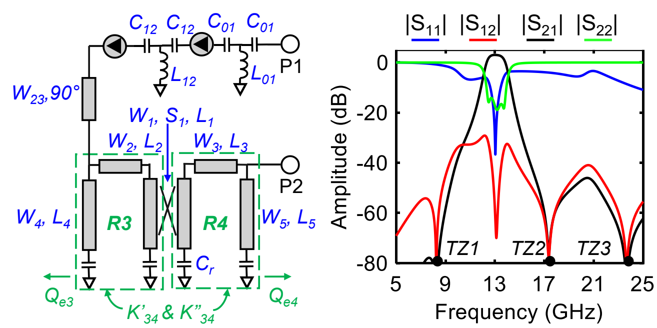

Fig. 7. (a) Circuit schematic of the four-stage BPFI. (b) Circuit-simulated S-parameters using: $C_{01} = 0.215$ pF, $L_{01} = 0.7$ nH, $C_{12} = 0.29$ pF, $L_{12} = 0.51$ nH, $W_{23} = W_1 = W_2 = W_3 = W_4 = W_5 = 120$ µm, $L_1 = 526$ µm, $S_1 = 2$ µm, $L_2 = 619$ µm, $L_3 = 835$ µm, $L_4 = 490$ µm, $L_5 = 274$ µm, $C_r = 0.41$ pF.

To develop the UFS using a commercially available 0.15 µm InGaAs process with two-metal layer stack-up, an E-mode pHEMT transistor (f_T = 113 GHz) is selected, and its key performance metrics, including maximum available gain (MAG) and minimum noise figure (NFmin), are analysed (Fig. 2). Using a baseline a gate biasing voltage of $V_g = 0.73$ V, a drain biasing voltage of $V_d = 3.3$ V, number of fingers (NOF) of 2, and unit gate width (UGW) of 25 µm, increasing the NOF results in higher NFmin with a slight reduction in MAG (Fig. 2(a)), whereas increasing the UGW raises both NFmin and MAG slightly (Fig. 2(b)). In all cases studied, the transistor's isolation ($|S_{12}|$) remains relatively constant at about 23 dB and is therefore omitted here for brevity. Following the UFS design methodology in [10], the transistor ensures UFS unilateral behaviour, with its NF directly impacting overall UFS's NF. For a balanced trade-off between gain and NF, the transistor was configured with NOF = 2, UGW = 25 µm.

After determining the transistor, resistors and an inductor are added in the transistor path and tuned for impedance matching and gain attenuation (to prevent oscillation), using the component values in Fig. 1. As shown in Fig. 3 (blue traces), the transistor-based path exhibits about 90° phase lead at 13 GHz in the forward direction. The coupled-line feedback

Table 1. Comparison with state-of-the-art active MMIC-based unilateral components

Ref.	Technology	Freq. (GHz)	D (dB)	$|S_{21}|$ (dB)	N/TZs	NF (dB)	IIP3 (dBm)	P_{DC} (mW)	Size (λ×λ)	Filt.
[5]	GaAs	8.6	30.6	-1.9	5/0	N.A.	20.4	228.6	0.034×0.233	Yes
[12]	GaAs	7.8	60	0-10	3/2	N.A.	0	100	N.A.	Yes
[13]	CMOS	24	36.8	-1.8	N.A.	6.7	14.8	3.6	0.053×0.035	No
[14]	SiGe HBT BiCMOS	5.5	30	-2	N.A.	13	0.7	5.4	0.011×0.008	No
T.W.	GaAs	13	30	-1.7	4/2	9.2	0.2	44	0.099×0.097	Yes

D: directivity; N: Number of transmission poles; Filt.: filtering.

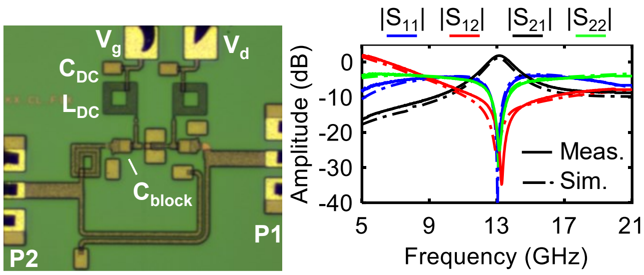

Fig. 8. (a) Photograph and (b) RF-measured and EM-simulated power transmission and reflection responses of the UFS.

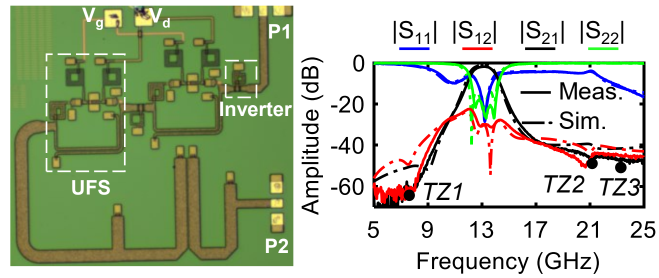

Fig. 9. (a) Photograph and (b) RF-measured and EM-simulated power transmission and reflection responses of the co-designed four-stage BPFI.

is then designed to introduce a 90° phase lag at 13 GHz (Fig. 3, red traces). Therefore, the RF signals in the UFS at the f_{cen}: i) constructively add in the forward direction (P1 to P2) due to the zero-phase loop formed by the feedback and the transistor paths (black trace in Fig. 1(b)), and ii) destructively add in the reverse direction (P2 to P1) due to the nearly 180° phase difference and balanced amplitude between the two parallel paths in this direction (red trace in Fig. 1(b)). Deviation from the center frequency disrupts this balance, resulting in a frequency-dependent power transmission response in the UFS.

To better demonstrate how different transistors and design parameters affect the overall performance of the UFS, design studies are provided in Fig. 4 and 5, with the premise of maintaining a directivity greater than 30 dB—a critical feature of the UFS. The impact of the transistor's NOF and UGW on the UFS performance is shown in Fig. 4. Increasing the NOF (Case 2 in Fig. 4(a)) or using a larger UGW (case 3 in Fig. 4(b)), while keeping the transistor's bias state, gain, BW, and directivity constant, results in an increase in the NF but also in enhanced IIP3. Additionally, the UFS can achieve higher gain by increasing the transistor's bias voltage, however at the expense of NF [see Fig. 5(a)]. Furthermore, as a frequency-selective stage, the BW of UFS can be adjusted by modifying the coupling factor (C) of the coupled-line feedback, as shown in Fig. 5(b). A wider BW, leads to improvements in both NF and IIP3, while reducing selectivity.

B. *Co-designed quasi-elliptic bandpass filter/isolator*

To realize BPFI responses with enhanced forward-direction selectivity and gain, alongside high reverse-direction isolation, the UFS can be cascaded with either additional UFSs or passive resonators. To facilitate their design using a diverse type of resonators while exploiting traditional filter synthesis method, the UFS is modelled using a CRD that can be represented by one resonating node (node 3') and three non-resonating nodes (nodes 1', 2', and 4') [4], as depicted in Fig. 6(a). Initial coupling element values for the transistor-based path are calculated using the design methodology in [4]. The feedback element, represented as $m_{1'4'}$, is selected to match the Y_{21} response of the actual coupled-line feedback at 13 GHz. Subsequent optimization refines these values with final parameters detailed in the caption of Fig. 6(a). A good agreement is observed between the circuit-simulated responses and the synthesized in Fig. 6(a), providing the foundation for synthesizing later high-order transfer functions in the BPFI.

To demonstrate the versatility of the BPFI design, an example design case of a BPFI comprising two UFSs and two reciprocal resonators is synthesized, as shown in Fig. 6(b), with the coupling values listed in the caption of Fig. 6(b). Mixed EM coupling between nodes 3 and 4 is used to introduce a TZ in CRD-synthesized responses of the four-stage BPFI in Fig. 6(b), with its position determined by $\Omega_{TZ} = -m'_{34}/m''_{34}$.

After specifying the CRD of the co-designed BPFI and its corresponding coupling values, the BPFI is implemented for f_{cen} of 13 GHz and 3-dB fractional bandwidth (FBW) of 12%. Its circuit diagram, shown in Fig. 7(a), is based on the UFS in Fig. 1(a) and two capacitively-loaded half-wavelength microstrip resonators designed on a GaAs MMIC platform. The coupling between the UFS and Port 1 (m_{01}) and between the UFS and the next UFS (m_{12}) are implemented by a high-pass T network, with LC values (e.g., for m_{01}) determined by (1).

$$C_{01} = \frac{m_{01}}{2 \cdot 50 \cdot \pi \cdot f} F,\; L_{01} = \frac{50}{2 \cdot \pi \cdot f \cdot m_{01}} H \qquad (1)$$

The coupling between the UFS and microstrip resonator R3 is realized using a quarter-wavelength inverter, with dimensions determined by the external quality factor Q_{e3}, which is related to m_{23} [11]. Besides, the mixed EM coupling m_{34} is implemented by partially coupling the two microstrip resonators, with the dimensions of the coupling defined by W_1, S_1, L_1 and determined by the desired denormalized inter-resonator coupling coefficients K'_{34} and K''_{34} related with m'_{34} and m''_{34} [11]. Finally, the coupling between microstrip resonator R4 and Port 2 is implemented by a direct connection between each other, with the connecting location determined by the desired external quality factor Q_{e4} related to m_{45} [11].

The simulated S-parameters of the BPFI are shown in Fig. 7(b). It exhibits three TZs (TZ1–TZ3) in the forward direction: TZ1 results from the mixed coupling between the resonators, while TZ2 and TZ3 originate from open-ended stubs (*L4* and *L5*) on the two sides of the microstrip resonators. As observed, the UFS in the co-design improves the power transmission from P1 to P2 while efficiently suppressing signals from P2 to P1. Compared to a single UFS, the co-designed BPFI provides higher selectivity and better out-of-band rejection, owing to the incorporation of reciprocal resonators and TZs.

III. Experimental Validation

To validate the proposed BPFI concept, prototypes of the MMIC-based Ku-band UFS and a four-stage BPFI were manufactured using a commercially available 0.15μm InGaAs process (PQG3-0C) from WIN Semiconductors. The photograph of the UFS is shown in Fig. 8(a), with measured RF performance alongside its corresponding EM simulated response provided in Fig. 8(b) demonstrating good agreement. At 13 GHz, biased with V_g = 0.69 V, V_d = 3.1 V, the UFS demonstrates a gain of 1.8 dB, directivity of 26 dB, NF of 7.9 dB, and IIP3 of 5.6 dBm. As for the four-stage BPFI, its photograph is shown in Fig. 9(a), and RF-measured performance is shown in Fig. 9(b), demonstrating a f_{cen} of 13 GHz, with a 3-dB FBW of 13%. Furthermore, it exhibits three TZs at 8 GHz, 21 GHz, and 22.8 GHz. When biased with V_g = 0.76 V, V_d = 2.02 V, it shows a gain of -1.7 dB, directivity of 30 dB, NF of 9.2 dB, and IIP3 of 0.2 dBm. Table 1 compares the proposed design with state-of-the-art active MMIC unilateral components. Unlike [13] and [14], which provide only isolator functionality, the proposed BPFI integrates both filtering and isolation capabilities. Compared to [5] and [12], it offers higher operating frequencies and reduced power consumption. Notably, it also obtains quasi-elliptic filtering responses due to the introduction of TZs, distinguishing it from [5].

IV. Conclusion

This paper presented the design and experimental validation of a Ku-band multi-functional RF component integrating quasi-elliptic bandpass filtering and isolation functionalities. It utilizes cascaded 0.15μm GaAs MMIC UFSs and passive resonators, enabling control over selectivity, directivity, and power transmission. A CRD-based design methodology was employed to integrate conventional coupled-resonator synthesis with the MMIC process. Prototypes of a UFS and a four-stage BPFI were fabricated and tested. The BPFI demonstrated a quasi-elliptic transfer function with four poles and three TZs, having -1.7-dB gain, 30-dB directivity, 9.2-dB NF, and 0.2-dBm IIP3 at 13 GHz.

Acknowledgment

This work was supported by Research Ireland under grants 20/RP/8334 and 13/RC/2077_P2. The authors would like to acknowledge WIN Semiconductors for manufacturing the devices.

References

[1] J. A. Zhang et al., "Enabling joint communication and radar sensing in mobile networks—a survey," *IEEE Commun. Surveys Tut.*, vol. 24, no. 1, pp. 306-345, First quarter 2022.

[2] K. E. Kolodziej, B. T. Perry and J. S. Herd, "In-band full-duplex technology: techniques and systems survey," *IEEE Trans. Microw. Theory Techn.*, vol. 67, no. 7, pp. 3025-3041, July 2019.

[3] S. M. Sifat, S. I. Shams and A. A. Kishk, "Millimeter-wave ferrite circulator integrated on gap waveguide technology," *IEEE Microw. Wireless Technol. Lett*., vol. 33, no. 8, pp. 1151-1154, Aug. 2023.

[4] A. Ashley and D. Psychogiou, "RF co-designed bandpass filters/isolators using nonreciprocal resonant stages and microwave resonators," *IEEE Trans. Microw. Theory Techn*., vol. 69, no. 4, pp. 2178-2190, Apr. 2021.

[5] A. Ashley and D. Psychogiou, "MMIC GaAs isolators and quasi-circulators with co-designed RF filtering functionality," *IEEE J. Microw*., vol. 3, no. 1, pp. 102-114, Jan. 2023.

[6] D. Simpson and D. Psychogiou, "Fully-reconfigurable non-reciprocal bandpass filters," *IEEE/MTT-S Int. Microw. Symp. Dig*., Aug. 2020, pp. 807-810.

[7] Z. Zhang and D. Psychogiou, "Incorporating directionality in transversal-resonator-based bandpass filters with tunable transfer function characteristics," *IEEE Trans. Circuits Syst. I, Regular Papers*, vol. 70, no. 12, pp. 5194-5207, Dec. 2023.

[8] K. Li and D. Psychogiou, "Multi-functional bandpass filters with frequency tunability and RF co-designed isolator functionality," in *Proc. 53rd Eur. Microw. Conf*., Sept. 2023, pp. 94-97.

[9] K. Li and D. Psychogiou, "Multifunctional and tunable bandpass filters with RF codesigned isolator and impedance matching capabilities," *Int. J. Microw. Wireless Technol*., pp. 1–15, 2024.

[10] K. Li and D. Psychogiou, "Tunable bandpass filters with co-integrated isolator and switching-off functionality," *IEEE J. Microw*., vol. 5, no. 1, pp. 190-206, Jan. 2025.

[11] J. S. Hong, *Microstrip Filters for RF/Microwave Applications*, 2nd ed. Hoboken, NJ, USA: Wiley, 2011.

[12] D. Simpson and D. Psychogiou, "MMIC active bandpass filter with nonreciprocal and quasi-elliptic response," *IEEE Microw. Wireless Technol. Lett*., vol. 33, no. 2, pp. 141-144, Feb. 2023.

[13] J. -F. Chang, J. -C. Kao, Y. -H. Lin and H. Wang, "Design and analysis of 24-GHz active isolator and quasi-circulator," *IEEE Trans. Microw. Theory Techn.*, vol. 63, no. 8, pp. 2638-2649, Aug. 2015.

[14] J. Lee, J. D. Cressler and A. J. Joseph, "A 5-6 GHz SiGe HBT monolithic active isolator for improving reverse isolation in wireless systems," *IEEE Microw. Wireless Compon. Lett*., vol. 15, no. 4, pp. 220-222, Apr. 2005.